






# Graphene-molecule-graphene single-molecule junctions to detect electronic reactions at the molecular scale

Chen Yang<sup>1,3</sup>, Caiyao Yang<sup>1,3</sup>, Yilin Guo<sup>1</sup>, Jianfei Feng<sup>1</sup> <sup>1</sup> and Xuefeng Guo<sup>1,2</sup> <sup>1,2</sup> 

**The ability to measure the behavior of a single molecule during a reaction implies the detection of inherent dynamic and static disordered states, which may not be represented when measuring ensemble averages. Here, we describe the building of devices with graphene-molecule-graphene single-molecule junctions integrated into an electrical circuit. These devices are simple to build and are stable, showing tolerance to mechanical changes, solution environment and voltage stimulation. The design of a conductive channel based on a single molecule enables single-molecule detection and is sensitive to variations in physical properties and chemical structures of the detected molecules. The on-chip setup of single-molecule junctions further offers complementary metal-oxide-semiconductor (CMOS) compatibility, enabling logic functions in circuit elements, as well as deciphering of reaction intermediates. We detail the experimental procedure to prepare graphene transistor arrays as a basis for single-molecule junctions and the preparation of nanogapped carboxyl-terminal graphene electrodes by using electron-beam lithography and oxygen plasma etching. We describe the basic design of a molecular bridge with desired functions and terminals to form covalent bonds with electrode arrays, via a chemical reaction, to construct stably integrated single-molecule devices with a yield of 30–50% per chip. The immobilization of the single molecules is then characterized by using inelastic electron tunneling spectra, single-molecule imaging and fluorescent spectra. The whole protocol can be implemented within 2 weeks and requires users trained in using ultra-clean laboratory facilities and the aforementioned instrumentation.**

## Introduction

The characterization of chemical reactions is typically based on the detection of ensemble-averaged atomic and bond parameters. However, to obtain a more accurate understanding of a single chemical reaction and how it differs from others requires characterizations at single-molecule resolution<sup>1,2</sup>. The major challenges faced in the field of single-molecule detection are the accurate capture of a single molecule and the precise detection of its weak signal. In response to these challenges, several single-molecule technologies have been developed, which can be mainly classified as optical<sup>3,4</sup>, mechanical<sup>5,6</sup> and electrical approaches<sup>7,8</sup>. Critical structural information of single molecules can be extracted from electrical measurements. One such approach is to monitor the obstructed ionic current by the passage of a molecule in a nanopore, with DNA sequencing as the most representative example<sup>9</sup>. Differing from detection methods based on molecular volume, shape and charge, measuring molecular conductance (typical scale of nanosiemens to microsiemens) stems from the molecular structure and therefore can provide information on the variations of configuration and conformation during a reaction<sup>7</sup>. Since the rectification property of one molecule with an electron donor– $\sigma$  bond–electron acceptor structure was initially proposed<sup>10</sup>, the field of molecular electronics has seen both experimental and theoretical developments<sup>11</sup>, with key developments such as the construction of molecular junctions including the selection of the electrode<sup>12</sup>, its interface<sup>13</sup> and the embedded molecule<sup>8,14</sup>.

Break junctions (BJs)—in which a junction between a molecule and an electrode is repeatedly formed and then subsequently broken by accurately controlling the movement of the electrode pair—can be formed between a scanning tunneling microscope (STM) probe and the substrate (STM-BJ)<sup>15,16</sup> or by what is referred to as a ‘mechanically controllable BJ’, in which the distance between metal

<sup>1</sup>Beijing National Laboratory for Molecular Sciences, National Biomedical Imaging Centre, College of Chemistry and Molecular Engineering, Peking University, Beijing, People’s Republic of China. <sup>2</sup>Centre of Single-Molecule Sciences, Institute of Modern Optics, Frontiers Science Centre for New Organic Matter, Tianjin Key Laboratory of Micro-scale Optical Information Science and Technology, College of Electronic Information and Optical Engineering, Nankai University, Tianjin, People’s Republic of China. <sup>3</sup>These authors contributed equally: Chen Yang, Caiyao Yang. ✉e-mail: [guoxf@pku.edu.cn](mailto:guoxf@pku.edu.cn)

electrode pairs can be accurately controlled directly on the substrate<sup>17</sup>. These two technologies provide the ability to characterize multiple single molecules in one experiment, making the results statistically relevant.

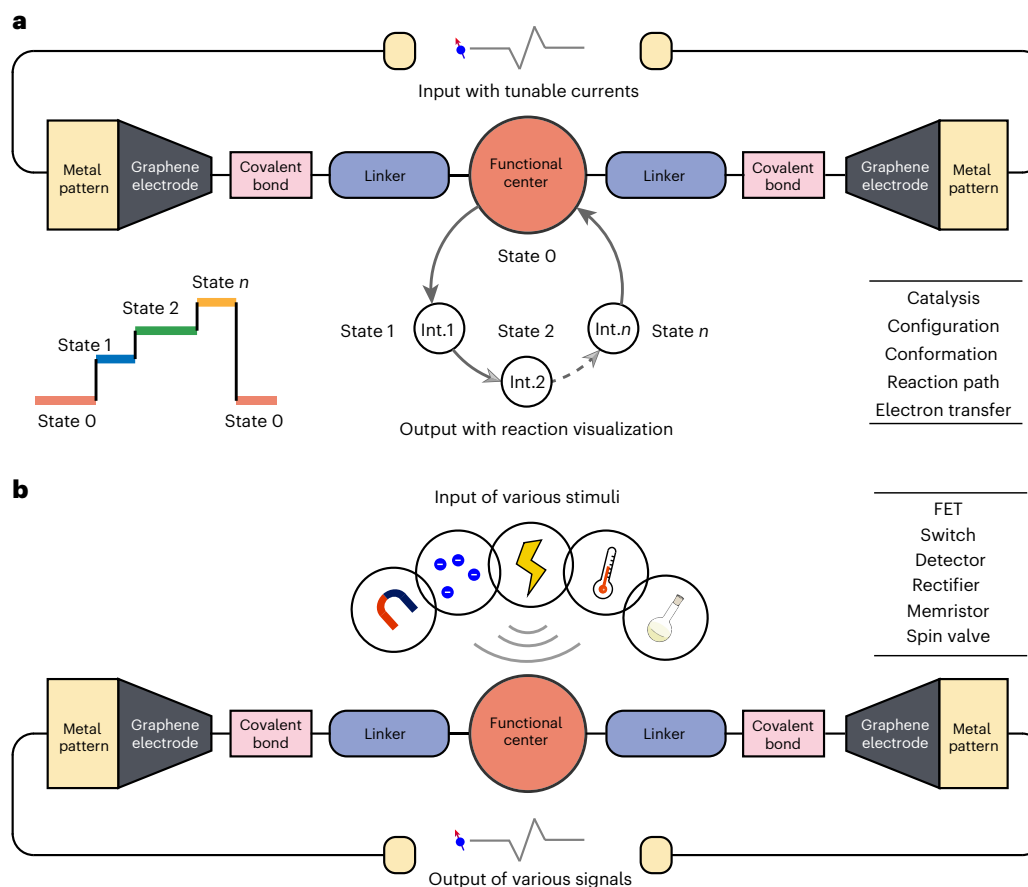
Single-molecule junctions (SMJs) with fixed electrodes may also be used. Although a statistically relevant representation of individual molecules cannot be achieved within one experiment (an issue that may be compensated for by preparing multiple junctions), the approach does allow for excluding the influence of the migration of the electrode atoms on the measured conductance, as well as for providing compatibility to complementary metal-oxide semiconductor-based equipment, and thereby provides accurate measurements. The measured conductance variations therefore mainly originate from the integrated molecular behaviors. The electromigration junction with metal electrodes<sup>18,19</sup> and the carbon-based SMJ (by  $\pi$ - $\pi$  stacking<sup>20–30</sup> or a covalent interface<sup>31</sup>) are two common types of junctions in which the electrodes are fixed on the substrate, and their nanogaps are prepared by electromigration or electroburning, respectively. The covalent interface of the graphene-molecule-graphene SMJs (GMG-SMJ) determines the interfacial coupling and tolerance to complex environments<sup>7</sup>. Since we first reported this technique in 2012<sup>31</sup>, the fabrication procedure has undergone many improvements, including supplementary electric burning<sup>32</sup> to improve the yield and allow for the use of alternative terminal groups of the molecular bridge, as well as improved characterizations of integrated molecules.

### Development of single-molecule devices and their application

We have developed carbon nanotube and graphene<sup>33,34</sup> single-molecule devices. In this protocol, we focus on the state-of-the-art GMG-SMJ, owing to their simpler fabrication procedure and higher success ratio (30–50% per chip, further identified by inelastic electron tunneling spectra (IETS), single-molecule imaging and fluorescent spectra; vide infra)<sup>35</sup>. The device enables probing of the mechanism in chemical reactions and biological processes by detecting single molecules. Because of the close relationship between molecular structure and conductance, the reaction trajectories of the embedded molecule are directly monitored by recorded currents, involving the detection of hidden intermediates (via conductance), visualization of the pathways (via conductance transformations) and thus clarification of the mechanism<sup>7</sup> (Fig. 1a).

Specifically, the noncovalent interactions between the molecule integrated between electrodes and the other surrounding molecules first characterized with our single-molecule device showed high electrical sensitivity to different interaction modes. For the intramolecular dynamics, the rotation of the C–C bond was detected by the current-voltage ( $I$ – $V$ ) scan according to stereoelectronic effect<sup>36,37</sup>. On the basis of this, the macroscopic aggregation-induced emission mechanism was further demonstrated by focusing on only one molecule, showing the capability to describe its dynamic stereostructures<sup>38</sup>. For the intermolecular interaction, the classical host-guest<sup>39</sup> and hydrogen-bond interactions<sup>40</sup> were recorded in in-situ current-time ( $I$ – $t$ ) curves according to the variations of the electron transmission in the conductive channel. For example, amino acids have the strong physiological activity to regulate the biological process, and their chirality allows their precise detection. To this end, we introduced cyclodextrin with natural chirality as a host in a molecular bridge to accurately distinguish different amino acids, as well as the corresponding enantiomers, and established a distinct ‘fingerprint database’ for chirality recognition<sup>41</sup>. In a different application, real-time monitoring of molecular machines (e.g., the rotaxane molecular shuttle) elucidates aspects of their structure, dynamics and operational mechanisms<sup>42</sup>. We also measured solvation by detecting ergodic interactions between the solvent and the embedded single molecule in the junction, illustrating microscopic heterogeneity in mixed alcohol-water solutions<sup>43</sup>. These nonbonded interactions are valuable to the functioning of biological systems and the preparation of bulk materials. However, we must note that single-molecule platforms are nevertheless model systems of ideal scenarios and may not accurately reflect the increasing complexity required to mimic biological functions.

Reaction mechanisms can also be deciphered by single-molecule devices. For a proof of concept, we detected the short-lifetime but inevitable carbocation intermediate during the  $S_N1$  nucleophilic substitution reaction based on a single 9-phenyl-9-fluorenyl center between electrodes, validating the feasibility of the single-molecule electrical platform with high temporal resolution (microseconds to milliseconds)<sup>44</sup>. Then, we further clarified the uncertain mechanism between two proposed pathways in Suzuki-Miyaura cross-coupling, by developing a single-molecule electrical spectroscopy<sup>45</sup>. This reaction was honored with the Nobel Prize in 2010 because of the efficient construction of C–C bonds by the palladium catalyzed coupling between aryl boronic acid (borate ester) and halogenated

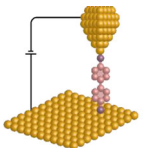
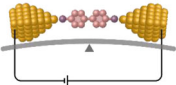
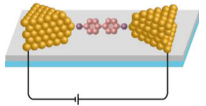
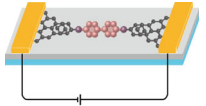
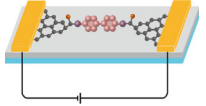


**Fig. 1 | Schematic illustrations of potential applications using single-molecule devices.** **a**, Representative implementation to reveal the reaction mechanism. With the input of tunable currents, the variations of the configuration, conformation and electron distribution of the focused single molecule can be accurately detected. The reaction path and catalytic process can be further described by the monitored current (inset) that reveals intermediate (Int.) states in a reaction. **b**, Representative strategies to construct multi-functional electrical devices. With the input of various stimuli (magnetic, electric and optical fields, temperature and chemical reagents) to the integrated molecule, different functional devices, such as a field-effect transistor (FET), switch, detector, rectifier, memristor and spin valve, can be realized at the single-molecule level.

aromatic hydrocarbons. However, whether the ligand exchange is required before transmetalation is not yet clear. Based on this electrical signal, the ligand-exchange-first pathway was determined as the predominant mechanism when visualizing reaction trajectories, clarifying the mechanism of Suzuki-Miyaura cross-coupling<sup>46</sup>.

The strong external electrical field (EEF) in nanogapped graphene electrodes provides opportunities to regulate the chemical reaction, especially processes involving polar transition states. For example, when two kinds of pericyclic reactions were monitored, they were affected by the EEF differently. When monitoring the Diels-Alder reaction, the traditional view is that both the new bonds are formed simultaneously. However, the time differences between the two bonds forming could be amplified by the EEF, and an intermediate state could be formed with only one of the bonds being detected, thus defining a stepwise pathway<sup>47</sup>. When monitoring the Claisen rearrangement, the allyl aryl ether rearrangement to produce allyl phenol was shown to migrate along the reaction coordinates with increasing EEFs according to the single-molecule kinetic isotope effect<sup>48</sup>. With the electrical input, the recorded signal could be used to obtain more information on matter transitions, involving unknown intermediates, transition states, quantum states and anomalous dynamic behaviors.

In addition to revealing underlying mechanisms, with the input of multiple stimuli, the electrical response can be measured as the output, meeting the demand for the miniaturization and multi-functionalization of electronic devices<sup>8</sup> (Fig. 1b). According to the close relationship between molecular orbital and electron transmission, applying a controllable stimulus to the molecule results in variations of the electrical properties. For example, the photoisomerization of the embedded molecule can constitute a type of photo-switching device<sup>34,49</sup>. The gate terminal induces high-performance current regulation by electrical field (on/off ratio up to  $10^4$ ), providing an insight into a

Single-molecule junction	Schematic	Features
Scanning tunneling microscope break junction		<ul style="list-style-type: none"> <li>• Super-resolution imaging available<sup>74</sup></li> <li>• Electrode distance controllable<sup>15</sup></li> <li>• Statistical significance of many molecules<sup>15</sup></li> <li>• Multiple anchor group candidates<sup>8</sup></li> </ul>
Mechanically controllable break junction		<ul style="list-style-type: none"> <li>• Electrode distance precisely controllable<sup>17</sup></li> <li>• Statistical significance of many molecules<sup>17</sup></li> <li>• Multiple anchor group candidates<sup>8</sup></li> </ul>
Electromigration junction		<ul style="list-style-type: none"> <li>• CMOS-compatibility<sup>18</sup></li> <li>• Multiple anchor group candidates<sup>8</sup></li> </ul>
$\pi$ - $\pi$ stacking graphene-molecule-graphene junction		<ul style="list-style-type: none"> <li>• CMOS-compatibility<sup>8</sup></li> <li>• Stability of electrodes to high voltages<sup>24</sup></li> </ul>
Covalent graphene-molecule-graphene junction		<ul style="list-style-type: none"> <li>• CMOS-compatibility<sup>8</sup></li> <li>• Complex solvent tolerance<sup>47</sup></li> <li>• Determined interface coupling<sup>8</sup></li> <li>• Stability to high voltages<sup>47</sup></li> </ul>

**Fig. 2 | A comparison of different single-molecule junctions.** A summary comparing the differences between single-molecule junction architectures<sup>8,15,17,18,24,47,74</sup>. CMOS, complementary metal-oxide-semiconductor.

miniaturized form of the electronic devices<sup>50,51</sup>. The introduction of EEF-induced asymmetry allows us to construct rectifiers at the single-molecule level<sup>52</sup>. In addition to these basic components in electrical circuits, the memristor and spin valve can also be developed by integrating different kinds of open-shell molecules. More functions can be expected to be realized by furthering our understanding of the quantum effect in a single molecule, such as those affecting electron transport<sup>53–55</sup>.

### Comparison with other single-molecule electrical approaches

Here, we focus on the comparison with other single-molecule electrical approaches. For a more detailed comparison with optical, mechanical and electrical nanopore single-molecule approaches, see the Supplementary Information. STM-BJs and mechanically controllable BJs show the ability to detect variations of the molecular structure<sup>34,56,57</sup>, configuration<sup>58</sup> and conformation<sup>16,59</sup> and enable molecular recognition<sup>60,61</sup> with statistical significance via repeated making and breaking of the junctions (Fig. 2). The molecule under analysis is typically designed with anchoring groups (the groups with lone electron pairs, such as  $-\text{SH}$ ,  $-\text{NH}_2$ ,  $-\text{PMe}_2$ , and  $-\text{NCS}^8$ ) that can more efficiently bind to metal electrodes.

Movable electrodes enable the formation of multiple SMJs in one experiment, whereas natural complementary metal-oxide semiconductor-compatible fixed electrodes focus only one molecule over a long time scale and exclude interference from electrode movement. Metal electrodes can also be adopted by electromigration and integrating molecules with the same anchors with BJs<sup>18,19</sup> (Table 1). A series of attractive molecular electrical properties have been discovered, which meet the requirements of the miniaturization and functionalization of electronic devices<sup>18,19</sup>. SMJs can also

be constructed by fixed carbon-based electrodes, such as carbon nanotubes<sup>33,62</sup> and graphene<sup>20–31,34,63–68</sup>. Graphene has a higher integration probability because of its inherent 2D structure, which has been adopted more experimentally. Based on the nanoscale gap formed on graphene by voltage pulses<sup>69</sup>, the subsequent molecular connection can be achieved by coupling to the underlying substrate<sup>65</sup>,  $\pi$ – $\pi$  stacking<sup>20–30</sup> or covalent bonding<sup>63</sup> (Table 1). The adoption of graphene as the electrode prevents the migration of metal atoms at high voltages. To expand the applicability in chemical reaction environments, the stable covalent interface has been further developed by our group. Carboxyl terminals on graphene are formed more efficiently via oxygen plasma etching<sup>70–72</sup> and then can integrate individual molecular bridges (with alternative terminals) via amide bonds. An additional benefit of oxygen plasma etching is the more defined geometry of the electrodes. This setup provides a tolerance in complex environments (wide temperature range and multiple solvents), determined interface coupling and biocompatibility. Long-term observation (scale of hours) of covalently embedded molecules opens up opportunities to detect one molecule at microsecond to millisecond time resolution. Note that once a covalent junction is formed, the integrated molecule cannot be removed or replaced. The suitability of the molecular bridge needs a priori consideration (e.g., the measurable conductance and the strength of the coupling between electrodes and the molecule), which can refer to the theory of molecular engineering based on our previous experimental evidence<sup>8</sup>. On the basis of this, a collection of molecular bridges with a certain functional center, spacer and anchor was established and successfully demonstrated the application for electronic devices and characterization of the chemical reaction.

Limitations of SMJ approaches include the effect by the natural electric field from the applied bias voltage between the source and drain terminals, which leads to electrostatic catalysis but can be quenched by the polar solvent. In turn, the electric field could be used to regulate the reaction and discover new phenomena. Another limitation is the unavoidable effect of other functional groups of the molecular bridge, as well as the electrode, on the focused reaction center through the covalently connected bonds. This limitation is weakened to some extent when adopting spacer groups like methylene. Furthermore, the time resolution needs to be improved. At present, the microsecond-to-millisecond time scale enables the monitoring of (sub) stable intermediate variations, and a picosecond-to-femtosecond resolution is the goal of future efforts to fully visualize chemical processes. Lastly, an aspect that warrants further research is how to extrapolate the behaviors detected in an SMJ to an Avogadro's number of molecules, taking into account that the increased complexity from a single molecule to molecular ensembles may affect the behavior of single molecules.

### Experimental design

We describe a procedure to prepare GMG-SMJ and their corresponding characterization. The basic part is the preparation of graphene field effect transistors (FETs) (Fig. 3). A single layer of high-quality graphene is grown on a copper sheet by high-temperature chemical vapor deposition (Fig. 3a,b). Graphene is first transferred to a polymethyl methacrylate (PMMA) film through spin coating and etching of copper substrates by using an FeCl<sub>3</sub> solution. The residual FeCl<sub>3</sub> can be removed by a hydrochloric acid solution followed by deionized water. The clean PMMA-supported graphene is then transferred to silicon wafers with 300-nm SiO<sub>2</sub> (suitable for characterization by microscopy). We can completely remove the PMMA by using acetone or annealing the chip by air or H<sub>2</sub> to obtain graphene on a chip. The shape of the graphene film can be further controlled by lithographic templates and oxygen plasma etching to form graphene point electrode arrays. First, the 40- $\mu$ m-wide strip is prepared by lithography (Fig. 3a,b), and then we use photolithographic patterning to apply, via thermal evaporation, a layer of chromium (8 nm) and gold (60 nm) on the strip to form the metal electrode arrays (source and drain, 12- $\mu$ m gap) (Fig. 3c). To prevent the current leaking into the solution phase, we evaporate 40-nm SiO<sub>2</sub> onto the metal electrodes. These graphene FET devices (Fig. 3d) are then ready to be characterized by the conductance measurement of every 20 pairs of gold electrodes (e.g.,  $I$ – $V$  scan). The conductance of  $G \geq 0.2$  mS shows good contact conductivity between graphene and metal electrodes.

An array of graphene electrode pairs with a range of gap-width distributions (1–10 nm) is designed to have more potential binding sites and achieve a higher probability for particular molecules to integrate (Fig. 4a). To prepare the array of graphene electrodes between each pair of gold electrodes (Fig. 4b; corresponding electrical characterization is provided in Fig. 4c), a dash-line pattern is designed with 150-nm length (210 intervals) and 5-nm width (considering the scattering of

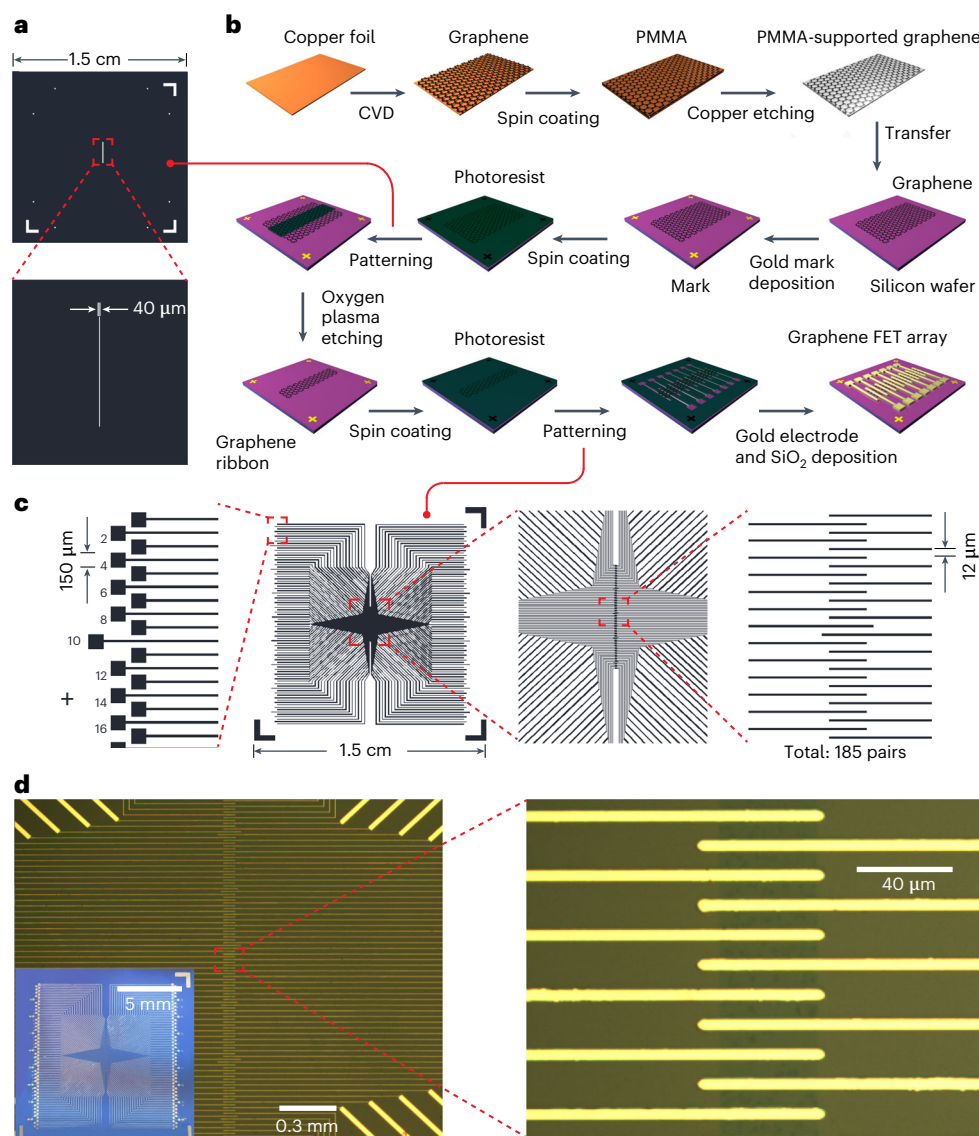


**Fig. 3 | Preparation of graphene FETs.** **a**, Pattern and corresponding enlarged image of the photolithographic mask to prepare the graphene ribbon by lithography (the black area for light transmission). **b**, Schematic diagram of the fabrication procedure, including the growth of the graphene, transferring graphene to the silicon wafer, the deposition of the mark for subsequent lithography, controlling the shape of the graphene and deposition of electrode arrays. **c**, Pattern and corresponding enlarged image of the photolithographic mask to prepare metal electrode arrays by lithography (the black area for light transmission). **d**, Optical images of the prepared graphene FETs (left) and of corresponding enlarged area (right). The inset shows the whole pattern, where the center is enlarged as shown in the left panel. The figure panels refer to Steps 1–82 of the procedure.

the electron beam and the intrinsically limited resolution of electron-beam lithography (EBL)) and prepared on pre-spin-coated PMMA by EBL (Fig. 4d,e). Graphene exposed from the dash-line window is then etched by oxygen plasma. By exploiting the gradual etching of PMMA and isotropic broadening, we can achieve narrow gaps with carboxyl terminals between indented graphene point contacts (Fig. 4f). The complete cutting of graphene electrodes can be characterized by the flat line in the  $I-V$  scan between the corresponding gold electrode pairs (Fig. 4g) in comparison with the case before cutting (Fig. 4b,c). The incompletely etched graphene in gold electrode pairs can be checked by  $I-V$  scan and broken by electroburning via Joule heating<sup>24</sup> to prepare nanogaps.

To integrate the molecular bridge with  $-NH_2$ ,  $-COOH$  or  $-N_3$  terminals into graphene electrode pairs, two kinds of procedures are proposed. For the  $-NH_2$  terminal<sup>73</sup>, freshly prepared graphene FET devices are immersed in a pyridine solution containing 0.1 mM molecular bridge and 1 mM 1-(3-dimethylamino-propyl)-3-ethylcarbodiimide hydrochloride. After 48 h, the devices are removed

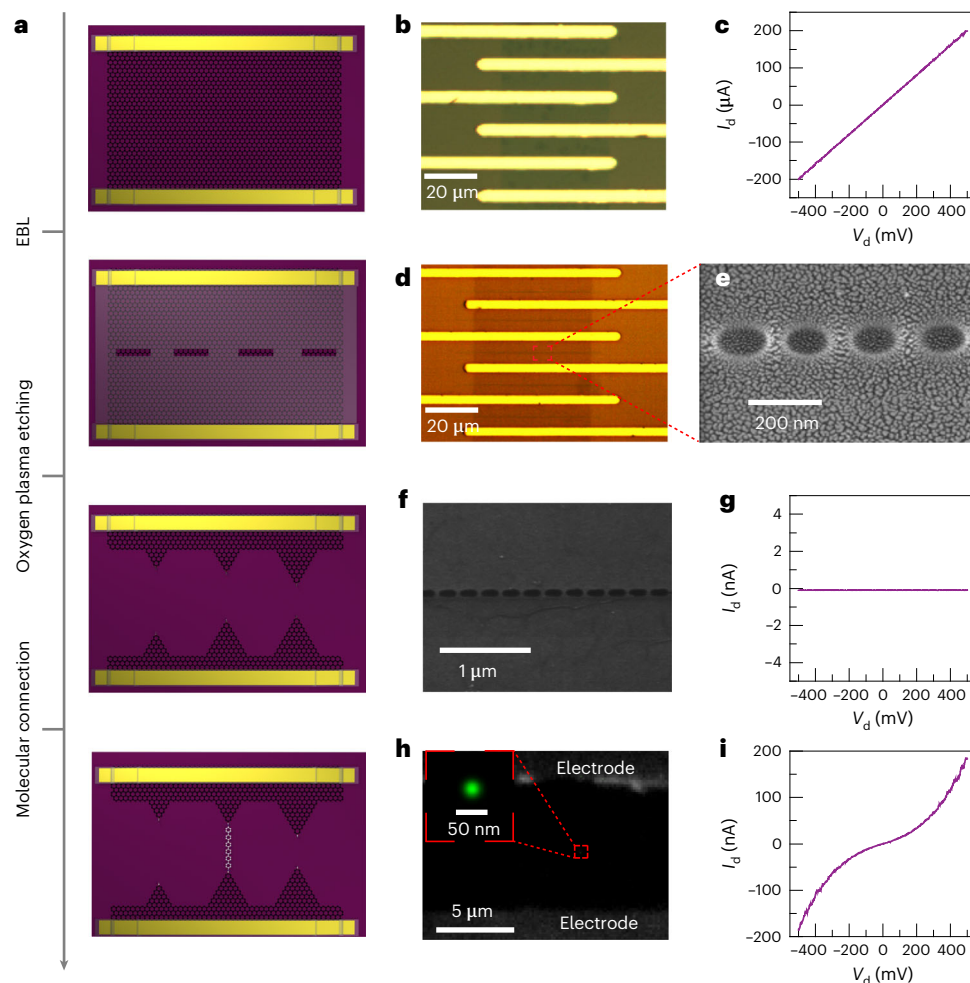


**Fig. 4 | Preparation of single-molecule devices.** **a**, Schematic diagram of the fabrication procedure. **b**, Photograph of the initial stage of graphene FETs. **c**, Corresponding  $I$ – $V$  scan between one pair of gold electrodes. **d**, Photograph of graphene FETs after EBL. **e**, Corresponding scanning electron microscopy image. **f**, Scanning electron microscopy image of the graphene electrode array after oxygen plasma etching. **g**, Corresponding  $I$ – $V$  scan between one pair of gold electrodes. **h**, Super-high-resolution image of the single-molecule site obtained by stochastic optical reconstruction microscopy. **i**,  $I$ – $V$  scan between one pair of gold electrodes after molecular connection. The figure panels refer to Steps 83–105 of the procedure.

from the solution, rinsed with deionized water and dried with flowing  $N_2$ . The  $-COOH$  terminal can be transferred to  $-NH_2$  via the pretreatment of *p*-phenylenediamine<sup>49</sup>. For the  $-N_3$  terminal<sup>46</sup>, we add  $10^{-3}$  M 2-hydroxydiphenylphosphinylbenzene, 1-ethyl-3-(3-dimethylaminopropyl) carbodiimide super-dried  $CH_2Cl_2$  solution, a catalytic amount of 4-dimethylaminopyridine and ethyldiisopropylamine (*i*-Pr<sub>2</sub>NEt) to the newly cut graphene device. The reaction is performed for 1.5 d under anhydrous and anaerobic conditions. After that, the device is removed and washed with ultra-dried  $CH_2Cl_2$  and ultra-dried tetrahydrofuran (THF). This step activates the carboxyl group with triphenylphosphine. A THF/ $H_2O$  (10:1) solution with  $10^{-4}$  M catalyst is added to the device with the reaction under anaerobic conditions for 1 d. Then, the device is removed, rinsed with THF and dried with flowing  $N_2$ . These two methods connect the molecular bridge between the graphene electrode pairs with amide bonds (Fig. 4h).

The successful connection can be characterized by recovery of the  $I$ – $V$  response between gold electrode pairs (Fig. 4i) (success yield: 30–50% on average). To further confirm the connection of the target molecular bridge, the IETS is introduced to characterize the vibration of involved chemical bonds in junctions according to electron–phonon coupling (Fig. 5). The single-molecule resolved spectrometer also provides information about the emission spectrum, including the molecular bridge and the product catalyzed by it (Fig. 5). We approach the characterization of individual molecule connections by using an integrated photo-electrical detection system. We use stochastic optical reconstruction microscopy

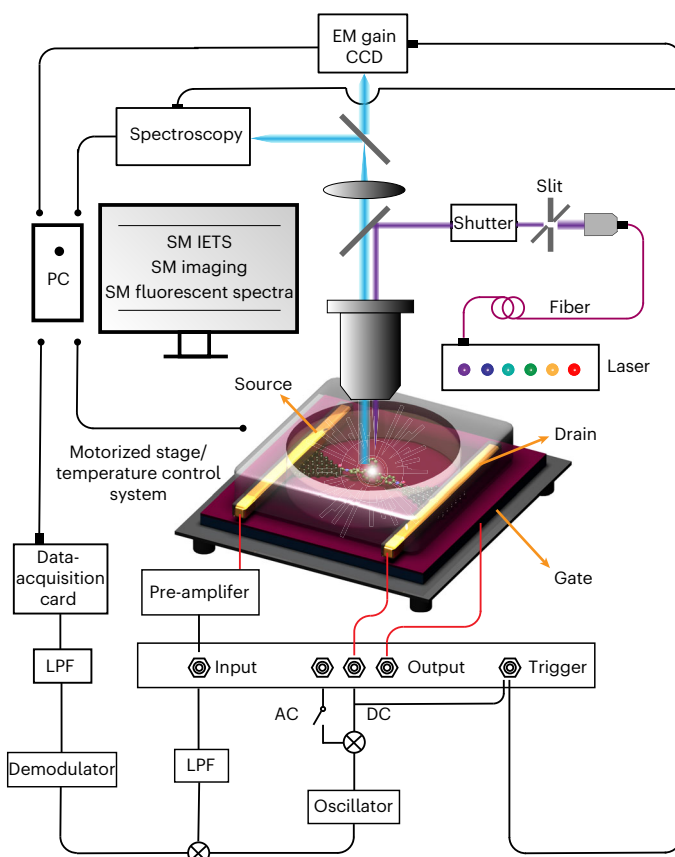


**Fig. 5 | Schematic diagram of the characterization system for single-molecule devices.** A pair of gold electrodes (source and drain) are connected to the input (by a pre-amplifier) and output terminals, respectively, of the lock-in amplifier to form a circuit. The modulated current through the single molecule (SM) can be demodulated to IETS and recorded. The gate can also be connected to the output terminal to obtain supernumerary regulation of the molecule. The trigger terminal is connected to the electron multiplier (EM) gain of the charge-coupled device (CCD) to synchronize the detection of optical and electrical signals. In addition, the optical signal can also be recorded by using single-molecule-resolved spectroscopy. LPF, low-pass filter; PC, personal computer.

(STORM) of the stochastic reaction (blinking) with a fluorescent molecule at the molecule site to image, at high resolution, the single molecule (Fig. 4h and Fig. 5), and the super-resolution microscopy data are integrated with electrical detection. The optical and electrical signals at the level of the individual molecule are in fact synchronous and strongly correlated with one another; therefore, by recording both, the results can be extrapolated to the single molecule, its location and characteristics.

### Expertise needed to implement the protocol

All the steps of device fabrications and single-molecule measurements should be conducted in a clean room. Facilities required to perform the characterization include an IETS (including a corresponding cryogenic setup, e.g., 2 K) and a STORM setup. Users with expertise in the use of these instruments are required.

## Materials

### Reagents

- Copper sheet (25 μm; Alfa Aesar)
- Hydrochloric acid (HCl; Xilong Scientific, cat. no. QC5791) **!CAUTION** HCl is a strong corrosive and irritant. Avoid skin and eye contact, ingestion and inhalation. Wear a face mask and acid- and alkali-resistant rubber clothing and gloves.
- Sulfuric acid (H<sub>2</sub>SO<sub>4</sub>; Xilong Scientific, cat. no. QC5782) **!CAUTION** H<sub>2</sub>SO<sub>4</sub> is a strong corrosive and irritant. Avoid skin and eye contact and ingestion. Wear a face mask and acid- and alkali-resistant rubber clothing and gloves.



- Hydrogen peroxide ( $\text{H}_2\text{O}_2$ ; Innochem, cat. no. 202460250) **!CAUTION**  $\text{H}_2\text{O}_2$  is a strong irritant. Avoid skin and eye contact and ingestion. Wear neoprene gloves.
- Acetone for analysis (HUSHI, cat. no. 80000367) **!CAUTION** Acetone is extremely flammable and is a strong irritant. Keep away from fire and heat sources. Ventilation should be maintained during use. Avoid skin and eye contact, ingestion and inhalation. Wear protective gloves and clothing, goggles and a mask.
- Absolute ethanol (Tong Guang, cat. no. 104022) **!CAUTION** Ethanol is extremely flammable and an irritant. Store in a cool, ventilated warehouse. Ventilation should be maintained during use. Avoid skin and eye contact, ingestion and inhalation. Wear protective gloves and clothing, goggles and a mask.
- Anhydrous ferric chloride ( $\text{FeCl}_3$ ; Xilong Scientific, cat. no. 13-1) **!CAUTION**  $\text{FeCl}_3$  is highly irritating. Avoid skin and eye contact, ingestion and inhalation. Wear protective gloves and clothing, goggles and a mask.
- Isopropyl alcohol (Concord Technology, cat. no. S6269) **!CAUTION** Isopropyl alcohol is highly flammable and an irritant. Store in a cool, ventilated warehouse. Ventilation should be maintained during use. Isopropyl alcohol may cause severe eye irritation and dizziness. Wear protective gloves and clothing, goggles and a mask.
- Methyl isobutyl ketone (MREDA, cat. no. M031383-100ml) **!CAUTION** Methyl isobutyl ketone is highly flammable and an irritant. Store in a cool, ventilated warehouse. Ventilation should be maintained during use. Avoid skin and eye contact, ingestion and inhalation.
- Pyridine (Alfa Aesar, cat. no. 043799) **!CAUTION** Pyridine is strongly irritating. Avoid skin and eye contact, ingestion and inhalation. Wear protective gloves and clothing, goggles and a mask.
- 1-Ethyl-3-(3-dimethylaminopropyl)carbodiimide hydrochloride (EDCI; 9dingchem, cat. no. D001F-25g) **!CAUTION** EDCI may cause skin irritation. Wear protective gloves and clothing, goggles and a mask.
- 2-Hydroxydiphenylphosphinylbenzene (Innochem, cat. no. H171138-100mg) **!CAUTION** Avoid skin and eye contact, ingestion and inhalation. Wear protective gloves and clothing, goggles and a mask.
- 1-Ethyl-3-(3-dimethylaminopropyl) carbodiimide (Bide Pharmatech, cat. no. BD10757-10g) **!CAUTION** Avoid skin and eye contact, ingestion and inhalation. Wear protective gloves and clothing, goggles and a mask.
- *i*-Pr<sub>2</sub>NEt (Energy-Chemical, cat. no. A01W3200141000) **!CAUTION** *i*-Pr<sub>2</sub>NEt is highly flammable and irritating. Avoid skin and eye contact, ingestion and inhalation. Wear protective gloves and clothing, goggles and a mask.
- Dichloromethane ( $\text{CH}_2\text{Cl}_2$ ; Innochem, cat. no. D3500) **!CAUTION** Avoid skin and eye contact. Wear protective gloves and clothing, goggles and a mask.
- THF (Concord Technology, cat. no. S6268) **!CAUTION** THF is highly flammable and irritating. Avoid skin and eye contact, ingestion and inhalation. Wear protective gloves and clothing, goggles and a mask.
- 4-Dimethylaminopyridine (Bide Pharmatech, cat. no. BD17199) **!CAUTION** Avoid skin and eye contact. Wear protective gloves and clothing, goggles and a mask.
- Polymethyl methacrylate (950 PMMA A5; Kayaku Advanced Materials Inc., cat. no. M230005 0500L 1GL) **!CAUTION** Avoid skin and eye contact. Wear protective gloves and clothing, goggles and a mask.
- Photoresist (Allresist GmbH, cat. no. AR-P 5350) **!CAUTION** Avoid skin and eye contact. Wear protective gloves and clothing, goggles and a mask.
- Developer (Allresist GmbH, cat. no. AR 300-26) **!CAUTION** Developer may be corrosive to metals. Avoid skin and eye contact. Wear protective gloves and clothing, goggles and a mask.
- Silicon wafer (Silicon Valley Microelectronics, Inc., cat. no. 0018147-006)
- Chromium slug (Beijing Licheng Innovation Metal Materials Technology Co., Ltd., cat. no. 20201116Cr001)
- Gold wire (ZhongNuo Advanced Material (Beijing) Technology Co., Ltd., cat. no. Au14503)
- Quartz disk (custom made, 2 cm × 6 cm; Chengtai Quartz Products Co., Ltd.)
- Bonding copper wire (Yesdo Electronic Materials (Yantai) Co., Ltd.)
- Silver glue (Jham Tech Co., Ltd., cat. no. SECrosslink 81V3)

### Reagent setup

#### Preparation of an $\text{FeCl}_3$ solution to etch the copper substrate

- 1 Add ~300 g of  $\text{FeCl}_3$  solid, 1 M hydrochloric acid solution (3 ml; prevent  $\text{FeCl}_3$  from hydrolyzing) and 500 ml of deionized water to the crystallization dish.
- 2 Dissolve the  $\text{FeCl}_3$  by sonication (power = 100 W, time = 50 min). The concentration of  $\text{FeCl}_3$  is ~3.7 M.
- 3 Filter to obtain the final corrosive solution.

### Preparation and disposal of the piranha solution

- 1 Prepare the piranha solution ( $\text{H}_2\text{O}_2:\text{H}_2\text{SO}_4$ , vol/vol = 3:7) by slow dropwise addition of 9 ml of  $\text{H}_2\text{O}_2$  (35% vol/vol) to 21 ml of concentrated  $\text{H}_2\text{SO}_4$  in a crystallization dish. **!CAUTION** The piranha solution is highly corrosive. To handle the piranha solution, use an acid-resistant laboratory coat, butyl gloves and chemical splash goggles.
- 2 Neutralize the remaining piranha solution by diluting it to a concentration of <10% in water. Then, slowly add a solution of NaOH or  $\text{Na}_2\text{CO}_3$  with stirring until the pH = 4–10.

### Preparation of a developer to develop the PMMA after EBL

Mix the methyl isobutyl ketone and isopropanol with a volume ratio of 1:3, and keep it in a refrigerator.

### Equipment

- Tube furnace (Thermo Scientific, cat. no. TF55035C-1)
- Resistance-heated evaporation coater (Beijing Technol, cat. no. ZHD300)
- Electron-beam evaporator (Beijing Technol, cat. no. TEMD500)
- Ultrasonic cleaning bath (Kunshan Hechuang, cat. no. KH-100DB)
- Spin coater (Schwan Technology, cat. no. EZ4)
- Heating plate (IKA, cat. no. C-MAG HP7)
- Optical microscope (Nikon, cat. no. eclipse lv100)
- Probe station (SUSS, cat. no. PM5)
- Semiconductor parameter system (Keysight, cat. no. B1500A)
- Pre-amplifier (DL, cat. no. 1211)
- Lock-in amplifier (Zurich Instrument, cat. no. HF2LI)
- UV lithography machine (45th Research Institute of China Electronic Technology Group, cat. no. BG-401A)
- Simplicity water-purification system (Sartorius, cat. no. arium 611DI)
- Reactive ion etching machine (Tailong Electronics)
- Field emission scanning electron microscope (FEI, cat. no. Nova NanoSEM 430)
- Fluorescence microscope (Nikon, Ni-E)
- Physical property measurement system (Quantum Design, DynaCool)

### Equipment setup

Tweezers for later use are sonicated in acetone, ethanol and deionized water for 15 min in turn. The thermal evaporation apparatus should be pre-wiped with ethanol.

## Procedure

### Preparation of graphene FETs ● Timing 1 week

#### Growth of graphene on copper sheets ● Timing 4 h

- 1 Place a tailored copper sheet (~2 cm × 6 cm) into a clean crystallization dish and add acetic acid until the copper sheets are submerged (20 min).
  - ▲ **CRITICAL STEP** The width (2 cm) of copper sheets should be moderate to match the diameter of the quartz tube of the furnace, and the length (6 cm) can be slightly longer. Keep the copper sheet surface as flat as possible during the process of tailoring the copper sheet to the required size (2 cm × 6 cm). Avoid any overlap between copper sheets; otherwise, it will affect the etching of the surface oxide layer. If the etching time is too short, the oxide layer on the surface will not be treated thoroughly; if the time is too long, the copper on the surface will be corroded.
- 2 Rinse the copper sheet three times with deionized water to remove acetic acid.
- 3 Rinse the copper sheet three times with absolute ethanol to remove water (easier to dry).
- 4 Dry the copper sheets with  $\text{N}_2$ .
- 5 Place the dried copper sheets in a desiccator for later use.
  - **PAUSE POINT** The sample (copper sheet) can be stored in a desiccator at room temperature for 1 month.
- 6 Place the quartz disk (~2 cm × 6 cm)-supported copper sheet into the chemical vaporization deposition (CVD) quartz tube.
- 7 Seal the CVD system to enable the subsequent vacuum pumping. The interface between the quartz tube and the pump is sealed with a vacuum clamp and a vacuum sealing ring.

- 8 Initiate the vacuum to  $<5$  Pa ( $\sim 1$  min) (Supplementary Fig. 1).  
**▲ CRITICAL STEP** The copper sheet should be placed close to the thermocouple to obtain an accurate temperature control. The distance ( $\sim 1$  cm) of the copper sheet migration by pump should be preconsidered and estimated (Supplementary Fig. 2).  
**? TROUBLESHOOTING**
- 9 Introduce  $H_2$  gas to the system with a flow rate of  $16\text{ cm}^3\text{ min}^{-1}$  (Supplementary Fig. 1).  
**! CAUTION** Check the air tightness of the whole system in advance to prevent hydrogen leakage and explosion.
- 10 Set the temperature control program: rise to  $1,040\text{ }^\circ\text{C}$  at a rate of  $0.5\text{ }^\circ\text{C/s}$  and keep at  $1,040\text{ }^\circ\text{C}$  for 1 h.  
**▲ CRITICAL STEP** The terminal temperature is just lower than the melting point of the copper sheet, to ensure the rearrangement and regularity of the surface atoms. This value varies between different CVD instruments.  
**! CAUTION** Beware of the high temperature.  
**? TROUBLESHOOTING**
- 11 Introduce  $CH_4$  gas to the system (Supplementary Fig. 1) with a flow rate of  $1.6\text{ cm}^3\text{ min}^{-1}$  and set the flow rate of  $H_2$  at  $8.0\text{ cm}^3\text{ min}^{-1}$ .
- 12 Keep the flow rate at  $8.0\text{ cm}^3\text{ min}^{-1}$  for 25 min (not including the first minutes of introduction) to grow graphene on the copper sheet.
- 13 Set the flow rates at  $16\text{ cm}^3\text{ min}^{-1}$  for  $H_2$  and  $0.8\text{ cm}^3\text{ min}^{-1}$  for  $CH_4$  and set the target temperature to the room temperature to cool.  
**▲ CRITICAL STEP** Keep  $CH_4$  to avoid the etching of grown graphene by  $H_2$ .
- 14 Turn off the  $CH_4$  source at  $700\text{--}800\text{ }^\circ\text{C}$ .
- 15 Turn off the  $H_2$  source below  $100\text{ }^\circ\text{C}$  (total cooling time:  $\sim 2$  h).
- 16 Close the pump and vent once it reaches a temperature  $<50\text{ }^\circ\text{C}$ , to take out the sample at room temperature ( $15\text{--}35\text{ }^\circ\text{C}$ ).  
**▲ CRITICAL STEP** Be careful to return the internal air pressure to atmospheric pressure and not to wrinkle the copper sheet because of excessive vented airflow or when removing the sample.  
**■ PAUSE POINT** The sample (graphene layer on the copper sheet) can be stored in a desiccator at room temperature for 1 month.

### Transfer of the graphene from the copper sheet to the silicon wafer ● Timing 20 h

- 17 Using a sharp pair of scissors, cut the copper sheet (graphene covered) into about six small pieces ( $\sim 2\text{ cm} \times 1\text{ cm}$ ).  
**▲ CRITICAL STEP** Choose a sharp pair of scissors to prevent wrinkling the copper sheet. Use tweezers for handling the copper sheet and do not touch the central section of the surface graphene (used for subsequent preparation of graphene electrodes). Pay attention to identifying the front (with graphene) and back face of the copper sheet during tailoring, because both faces look the same.
- 18 Place the copper pieces on supports to further spin coat.  
**▲ CRITICAL STEP** The clean cut-offs from the silicon wafer ( $\sim 1.5\text{ cm} \times 1.5\text{ cm}$ ) usually make good supports.
- 19 Place the copper piece (along the long side) face up in the center of the chosen silicon wafer (Supplementary Fig. 3).  
**▲ CRITICAL STEP** Keep flat but do not stretch the copper sheet.
- 20 Set the spin coater at  $4,000\text{ rpm}$  for 45 s.
- 21 Fix the silicon wafer-supported copper sheet on the rotor.  
**▲ CRITICAL STEP** Make sure that the silicon wafer is firmly fixed to prevent it from disengaging during rotation.
- 22 Add PMMA 950 (anisole solvent) dropwise to the sample surface and start the spin-coating program. Because of the contamination and evaporation of anisole from the mouth of the dropper, discard the first two drops with each addition.  
**▲ CRITICAL STEP** PMMA 950 is added dropwise just to cover the copper piece. Too little will lead to unsatisfactory coverage, and too much will stick the copper piece to the silicon wafer.
- 23 Remove the samples from the spin coater.
- 24 Heat the samples at  $180\text{ }^\circ\text{C}$  for 2 min on a hot plate to remove the anisole solvent.
- 25 Remove the copper pieces (by using tweezers) from the supported silicon wafer and place them in a clean Petri dish face up.

▲ **CRITICAL STEP** Be careful to avoid wrinkling the copper piece, especially in the presence of excessive PMMA between the copper piece and silicon wafer.

- 26 Use oxygen plasma etching (reactive ion etching machine, detailed parameters: power = 50 W, time = 60 s, oxygen flow rate = 40 standard cubic centimeters per minute (SCCM), total pressure = 15 Pa) to remove the graphene and contamination on the back face of the copper pieces.

#### Preparation of the silicon wafer substrates

- 27 Cut the silicon wafer by using a diamond scribe to the desired size (e.g., 1 cm × 1 cm, 1.5 cm × 1.5 cm and 1.8 cm × 3.5 cm). This step requires multiple cuts.

▲ **CRITICAL STEP** Before each cut, use a suction ball to blow away the residual particles on the surface.

- 28 Place the cut silicon wafers into the piranha solution and heat it at 110 °C for 2–3 h until no air bubbles emerge.

▲ **CRITICAL STEP** Avoid overlapping the silicon wafers; otherwise, it will affect the surface cleanliness, and the surfaces may be scratched by each other.

- 29 Remove the piranha solution and add ~50 ml of deionized water, followed by three periods of ultrasonic cleaning (10 min each period).

- 30 Dry the wafers by flowing N<sub>2</sub> in an ultra-clean platform.

- 31 Seal the wafers in a Petri dish by using Parafilm for later use.

■ **PAUSE POINT** The sample (silicon wafer) can be stored in a Petri dish at room temperature for 1 month.

#### Etching of the copper substrate

- 32 Place the sample (PMMA/graphene/copper, PMMA face up) into the surface of the etching solution for 2 h until complete etching.

▲ **CRITICAL STEP** Make sure that the sample floats on the surface of the etchant, and do not immerse the sample. If the etching time is too short, the copper removal will be incomplete.

#### ? TROUBLESHOOTING

##### Rinsing of the PMMA-supported graphene

- 33 Pick up the samples (PMMA membrane) with a slightly larger prepared silicon wafer (Step 31), and put them floating in a 0.1 M hydrochloric acid solution and wait for 0.5 h.

▲ **CRITICAL STEP** Keep the PMMA film flat and avoid wrinkling.

- 34 Transfer the PMMA membrane to the surface of 0.05 M hydrochloric acid and deionized water in turn by using a larger silicon wafer, and wait for 0.5 h, respectively.

- 35 Transfer the PMMA membrane to a 1 M KOH solution in the same way, followed by 0.5 h of waiting.

▲ **CRITICAL STEP** KOH should be completely dissolved by sonication.

- 36 Transfer the PMMA membrane to the surface of deionized water, 0.05 M hydrochloric acid and deionized water in turn by using a larger silicon wafer, and wait for 0.5 h, respectively.

- 37 Transfer the PMMA membrane to the surface of deionized water by using a larger silicon wafer and wait for 1 h.

- 38 Pick up the PMMA membrane with the prepared silicon wafers (Step 31) and place it in the center of the silicon wafer surface.

▲ **CRITICAL STEP** Use a needle to assist in picking up and position adjustment; be careful not to poke into the middle of the PMMA membrane (Supplementary Fig. 4).

- 39 Heat a hot plate at 40–50 °C to remove water until complete removal of the residual water (~1 h).

- 40 Determine whether the water between the silicon wafer and the sample is completely evaporated by examining the color of the PMMA membrane (colorless to red or green).

▲ **CRITICAL STEP** If the temperature is too high and the evaporation is too fast, air bubbles will be formed, resulting in the fragmentation of graphene. If the time is too long, the film will shrink, and the graphene–wafer interaction will be weak; if the time is too short, there will be residual moisture between the silicon wafer and PMMA/graphene, which will cause the final transferred graphene to be broken.

#### ? TROUBLESHOOTING

- 41 Place the dry sample in a quartz tube of a CVD furnace, introduce a mixture of argon (0.6 SCCM) and H<sub>2</sub> (0.6 SCCM), and anneal it at 420 °C for 1 h to obtain a silicon wafer–supported graphene.

- 42 Remove the sample after cooling down to room temperature (set the target temperature at 30 °C and leave it to cool for ~3 h). The atomic force microscopy (AFM) image shows the flatness of graphene (Supplementary Fig. 6).  
**! CAUTION** Beware of hydrogen leakage at high temperature.

### ? TROUBLESHOOTING

#### Deposition of the mark on the graphene-silicon wafer ● Timing 5 h

- 43 Turn on the spin coater.  
44 Fix the graphene wafer on the rotor by vacuum suction.  
45 Drip the photoresist on the surface of the silicon wafer.  
46 Start the spin coating (4,000 rpm for 45 s).  
47 Place the wafer on a preheated hot plate (110 °C) for 3 min.  
**▲ CRITICAL STEP** Make sure that the photoresist just completely covers the silicon wafer. Too much photoresist may contaminate the vacuum stage and even block the vacuum line system of the spin coater, but too little will not cover all the surface.

### ? TROUBLESHOOTING

- 48 Turn on the lithography instrument, UV light source, vacuum pump and main valve of the gas cylinder.  
49 Load the mark mask according to the instructions on the screen.  
50 Place the silicon wafer in the center of the sample stage and expose it for a certain time (16 s for the UV lithography machine listed above).  
**▲ CRITICAL STEP** Make sure that the lithography patterns are all within the scope of the silicon wafer; otherwise, all the marks cannot be obtained in the future.  
51 After lithography, the silicon wafer is taken out by using tweezers and placed into the developer (30 ml) (Allresist GmbH, cat. no. AR 300-26) for 15 s.  
52 Take the sample out from the developer by using tweezers and place it into deionized water (30 ml) for 15 s to stop the developing.  
53 Dry with flowing N<sub>2</sub>. All the obtained lithographic cross-marks are clearly visible under a 20× optical microscope.  
54 Attach the sample (graphene on silicon substrates) to the glass substrate, transfer it to a thermal evaporation apparatus prepiped with ethanol and vacuum to  $\sim 5 \times 10^{-5}$  Pa.  
55 The chromium evaporation source is heated via increasing the heating current (turn the corresponding knob) to ~20 A at the ammeter. Keep this status (near the evaporation temperature) for a short time (~1 min) to remove surface impurities.  
56 The gold evaporation source is heated via increasing the heating current (turn the corresponding knob) to ~120 A at the ammeter. Keep this status (near the evaporation temperature) for a short time (~1 min) to remove surface impurities.  
57 Remove the shutter located in front of the sample by using the mechanical knob.  
58 Electrically heat the chromium evaporation source again and deposit 8-nm chromium at a rate of 1 Å/10 s.  
59 Electrically heat the gold evaporation source again and deposit 60-nm gold at a rate of 1 Å/10 s.  
**▲ CRITICAL STEP** Avoid fast deposition, to avoid poor adhesion of the mark to the silicon wafer.  
**? TROUBLESHOOTING**  
60 Immerse the deposited wafer in acetone for 10 min.  
61 Rinse off the photoresist outside the mark with fresh acetone.  
62 Blow dry with flowing N<sub>2</sub> for 10 s.

#### Preparation of graphene ribbons ● Timing 2 h

- 63 Turn on the spin coater and corresponding pump.  
64 Fix the graphene wafer on the rotor by vacuum suction.  
65 Drip the photoresist on the surface of the silicon wafer.  
66 Start the spin coating (4,000 rpm for 45 s).  
67 Place the wafer on a preheated hot plate (110 °C) for 3 min.  
**▲ CRITICAL STEP** Make sure that the photoresist just covers the center of the silicon wafer. The ribbon pattern is limited only to the center of the wafer.

- 68 Turn on the lithography instrument, UV light source, vacuum pump and main valve of the gas cylinder and load the ribbon mask (designed by the L-edit software) according to the instructions on the screen. Align the marks on the wafer exactly with the marks on the mask and expose it to UV for a certain time (16 s for the UV lithography machine listed above).  
**▲ CRITICAL STEP** Ensure complete alignment; otherwise, it will affect subsequent accurate loading of metal electrodes.
- 69 After lithography, the silicon wafer is taken out and developed with the special developer (Allresist GmbH, cat. no. AR 300-26) for 15 s, fixed with deionized water for 15 s and dried with flowing N<sub>2</sub>. The obtained photoresist ribbon is clearly visible under a 50× optical microscope.
- 70 The developed devices are etched with oxygen plasma for 60 s. Rinse the remaining photoresist on the surface with acetone and then blow dry with N<sub>2</sub>. The obtained graphene ribbon is clearly visible under a 50× optical microscope.

### Preparation of metal electrodes ● Timing 5 h

- 71 Turn on the spin coater, fix the graphene-ribbon device, drip the photoresist on the surface of the silicon wafer, start spin coating (4,000 rpm for 45 s) and place the wafer on a preheated hot plate (110 °C) for 3 min.  
**▲ CRITICAL STEP** Make sure that the photoresist just completely covers the silicon wafer. Too much photoresist may contaminate the vacuum stage and even block the vacuum line system of the spin coater, but too little will not cover all the surface.
- 72 Turn on the lithography instrument, UV light source, vacuum pump and main valve of the gas cylinder and load the electrode mask according to the instructions on the screen. Align all the marks on the wafer exactly with the marks on the mask and expose it to UV for a certain time (16 s for the UV lithography machine listed above).  
**▲ CRITICAL STEP** Ensure accurate alignment; otherwise, it will cause displacement between the electrode and the graphene strip.
- 73 After lithography, the device is taken out and developed with the special developer (Allresist GmbH, cat. no. AR 300-26) for 15 s, fixed with deionized water for 15 s and dried with flowing N<sub>2</sub>. The obtained electrode pattern is clearly visible under a 50× optical microscope.  
**▲ CRITICAL STEP** Ensure complete development (the underlying graphene or silicon wafer should be clearly visible by using a microscope); otherwise, a poor interface contact between electrodes and graphene will result.
- ? TROUBLESHOOTING**
- 74 Attach the device to the glass substrate, transfer it to a thermal evaporation apparatus prepiped with ethanol and vacuum to  $\sim 5 \times 10^{-5}$  Pa.
- 75 The chromium and gold evaporation sources are sequentially heated to near the evaporation temperature for a short time (~1 min) to remove surface impurities.
- 76 Electrically heat the chromium evaporation source and deposit 8-nm chromium at a rate of 1 Å/20 s.
- 77 Electrically heat the gold evaporation source and deposit 60-nm gold at a rate of 1 Å/20 s.  
**▲ CRITICAL STEP** Too fast deposition will lead to poor adhesion of the electrodes to the silicon wafer and graphene.
- 78 Deposit 40-nm SiO<sub>2</sub> by electron beam evaporation at a rate of 0.1 nm/s.
- 79 Immerse the deposited device in acetone for 30 min.
- 80 Rinse off the photoresist outside the electrodes with fresh acetone.
- 81 Blow dry with flowing N<sub>2</sub>. The prepared graphene FET should be clearly visible under a 50× optical microscope (Fig. 3d, right panel).
- 82 Measure the current among each 20 pairs of electrodes under 50-mV bias voltage by using a PM5 probe station. The anticipated current should be  $\geq 6 \mu\text{A}$ .

### ? TROUBLESHOOTING

### Preparation of the single-molecule device ● Timing 5 d

#### Opening of windows on PMMA layers ● Timing 4 h

- 83 Spin-coat a PMMA layer (4,000 rpm for 45 s) on the surface of electrically characterized devices.
- 84 Heat the devices at 180 °C for 2 min on a hot plate.

- 85 Poke holes with a needle tip in the PMMA layer near the ends of the graphene ribbon on the probe station for subsequent electron microscope focusing (Supplementary Fig. 5).
- 86 Put the sample into the cavity of the EBL system, and set the high voltage to 30 kV when the cavity pressure is lower than  $10^{-5}$  torr.  
**▲ CRITICAL STEP** Make sure that the back of the sample is clean, to avoid uneven sample sticking; otherwise, it will cause an uneven pattern.
- 87 Set a suitable working distance (5 mm for the scanning electron microscope listed above) and adjust the image clearly through alignment, astigmatism and focusing functions.  
**▲ CRITICAL STEP** Make sure that the image is clear when changing the working distance, to avoid the sample stage hitting the pole piece.
- 88 Call up the designed CAD file by using the ELPHY Plus software, and set the patterning parameters. For the EBL system listed above, the suitable beam current is 0.17 nA, and the area dose is  $2,600 \mu\text{C}/\text{cm}^2$ .
- 89 Move the sample stage in the horizontal direction and open windows on PMMA with EBL; the designed CAD file consists of three 5-nm-width dash lines (each window is 150 nm long, with 40 nm between windows).
- 90 Check the lithographic position every three to four scans. If offset, adjust the position to the middle of the electrode pair.  
**▲ CRITICAL STEP** A working distance of 5 mm should be maintained throughout the lithography, so refocusing should be done before exposing the next graphene ribbon. The size and spacing of the windows are critical for obtaining satisfactory graphene nanogaps and should be strictly observed. See the systematic exploration in ref. <sup>31</sup> for details.
- 91 Develop the device in the developer at 5 °C with the aid of sonication. Every 10 s, wash it in a fixing bath (isopropanol) and dry it under a gentle  $\text{N}_2$  flow.  
**▲ CRITICAL STEP** High ultrasonic power can lead to poor adhesion of the metal electrode to the substrate. A single development (lasting 15–20 s) is recommended, because a back-and-forth 10-s development may cause deviation of the developing pattern from the exposure pattern.
- 92 Observe the etching lines with an optical microscope. The standard for judging appropriate development is that the etching line between each pair of electrodes is faintly visible at 20× magnification and clearly visible at 50× magnification.

## ? TROUBLESHOOTING

### Cutting of graphene ribbons by oxygen plasma ● Timing 3 h

- 93 Place the device from Step 92 in the reactive ion etching (RIE) machine and cut the graphene through the open windows by oxygen plasma (15 Pa, 50 W power) (the corresponding AFM image refers to Supplementary Fig. 7a). After each cutting, measure the electrical conductivity between every 20 pairs of electrodes.  
**▲ CRITICAL STEP** A single oxygen plasma cut is recommended (cutting time = 20 s), and the cutting yield is controlled to 50–60% (no current response to the bias voltage).  
**? TROUBLESHOOTING**
- 94 A piece of paper should be used to cover the severed section to prevent over-etching before full cutting of the whole electrode pair array on the chip.
- 95 Immerse the device in acetone for ~30 min to remove the residual PMMA.
- 96 Dry it with  $\text{N}_2$  for 10 s.

### Supplementary cutting of graphene ribbons by electroburning ● Timing 2 h

- 97 Measure the conductivity of each pair of electrodes in turn. A current of <5 pA ( $V_d = 1.0$  V) indicates that the graphene between the electrodes has been cut off by oxygen plasma.
- 98 Apply the method of electroburning for the incompletely etched graphene, and set the single voltage sweep ranging from 0 to 20 V, with a sweep rate of 20 mV/s and a sampling rate of 10 samples/s.
- 99 Stop applying the voltage when the current rapidly drops to picoampere scale.
- 100 Repeat the  $I$ – $V$  scans to ensure a femtoampere-to-picoampere-scale current at 1 V to fully open the gap (the corresponding AFM image refers to Supplementary Fig. 7b). The graphene nanoconstriction arrays can be burned off at the small bias and current. The critical current region of most electroburning processes is 6–300  $\mu\text{A}$ , and the critical voltage region is 2–3 V. The typical

*I*-*V* curves of incompletely cut graphene are provided in Supplementary Fig. 8, which should be excluded when characterizing the single-molecule connection (vide infra).

? TROUBLESHOOTING

**Reconnection of graphene point contacts by molecules** ● **Timing 3 d**

101 The following methods can be adopted to integrate molecules into graphene nanoelectrodes, depending on the functional groups at the end of the molecular bridge.

(A) **Procedure for the connection of –NH<sub>2</sub> and –OH terminal molecules**

- (i) Immerse the device from Step 100 in pyridine with a molecular concentration of 10<sup>-4</sup> M.
- (ii) Add 10–15 equivalents (molar ratio) of EDCI to react for 2 d in an argon atmosphere.  
■ PAUSE POINT The device can be stored in an argon atmosphere at room temperature for 2 d.

(B) **Procedure for the connection of –COOH terminal molecules**

- (i) Immerse the device from Step 100 in pyridine containing *p*-phenylenediamine at a concentration of 10<sup>-4</sup> M.
- (ii) Add 10 equivalents (molar ratio) of EDCI to react for 1 d in an argon atmosphere.
- (iii) Remove the device from solution and clean it with water and acetone.
- (iv) Immerse the device in pyridine with a molecular concentration of 10<sup>-4</sup> M, and add 10 equivalents (molar ratio) of EDCI to react for 2 d in an argon atmosphere.  
■ PAUSE POINT The device can be stored in an argon atmosphere at room temperature for 2 d.

(C) **Procedure for the connection of –N<sub>3</sub> terminal molecules**

- (i) Immerse the device from Step 100 in 1-ethyl-3-(3-dimethylaminopropyl) carbodiimide super-dried CH<sub>2</sub>Cl<sub>2</sub> containing 2-hydroxydiphenylphosphinylbenzene at a concentration of 10<sup>-3</sup> M.
- (ii) Add a catalytic amount of 4-dimethylaminopyridine and *i*-Pr<sub>2</sub>NEt to react for 1.5 d under anhydrous and anaerobic conditions.
- (iii) Remove the device and wash it with ultra-dried CH<sub>2</sub>Cl<sub>2</sub> and ultra-dried THF.
- (iv) Immerse the device in THF/H<sub>2</sub>O (10:1) solution with a molecular concentration of 10<sup>-4</sup> M to react under anaerobic conditions for 1 d.  
■ PAUSE POINT The device can be stored in an argon atmosphere at room temperature for 1 d.

102 After the reaction, carefully wash the device with deionized water and acetone in turn to remove the residual solvent and by-product.

103 Dry it under a gentle N<sub>2</sub> flow (<0.1 Mpa).

104 Once it is dry, place the device in a metal box to shield it from static electricity.

■ PAUSE POINT The device can be stored in a metal box for 2 years.

105 Measure the *I*-*V* curve of each pair of electrodes, and the bias voltage scanning range is ± 0.5 V. Transition from the original open circuit to the conducting state indicates that the molecule is successfully connected. The *I*-*V* scans of all the electrode pairs (integrating two kinds of molecules) on two chips are provided in Supplementary Fig. 9.

▲ CRITICAL STEP Wearing antistatic clothing and a wristband is recommended during the measurement.

106 Characterize the properties of the integrated molecule

(A) **Optically, by super-resolution optical imaging**

- (i) Place the device on the motorized stage of the microscope.
- (ii) According to the above electrical test, find the target metal electrode pair (*I*-*V* response) under the 10× objective lens by moving the motorized stage.
- (iii) Switch to the 100× objective lens and focus the device clearly.
- (iv) Set the exposure time (usually 100 μs–50 ms), the gain of the camera (usually 300–500) and the number of photos (usually 3,000–5,000).
- (v) Perform stochastic optical reconstruction in NIS-element software after collection.

(B) **Measuring the IETS of the integrated molecule at 2 K**

- (i) The electrode patterns (source and drain) are wire-bonded to the specific circuit board by copper wires and the silver glue. After drying the silver glue, the electric characteristics are measurable via the bonded circuit board.



- (ii) Place the circuit board with the device in the cavity of a physical property measurement system and connect it to outside circuits (the input and output terminals of the lock-in amplifier, respectively; Fig. 5).
- (iii) Set the temperature to 2 K after pumping.
- (iv) The second harmonic in the  $I-V$  scan (direct current mode) with (prime-number frequency) alternating current loading is demodulated, which is the IETS. The applied AC modulation voltage is selected in the range of 5–20 mV (rms value), depending on the signal strength. The low-pass filter bandwidth is  $\sim 3$ –10 times the modulation frequency.

## Troubleshooting

Troubleshooting advice can be found in Table 1.

Step	Problem	Possible reason	Solution
8	Migration of the copper sheet beyond the supported quartz disk	The air flow of pumping	Place -1 cm ahead in the opposite direction of airflow
10	Temperature value varies between different CVD instruments	Inherent instrument error	Test the actual temperature with a thermocouple and then calibrate the temperature
32	Incomplete etching of copper	Too much PMMA dripping during spin coating	Add PMMA dropwise to just cover the copper piece before spin coating
40	Residual moisture between the silicon wafer and the PMMA membrane	The time of evaporation is too short	Wait for the PMMA membrane to change from colorless to red or green
42	The PMMA membrane separated from the silicon wafer	The membrane shrinks because of long-time evaporation	Once the membrane changes from colorless to red or green, the next step should be started
42	Fragmentation of the transferred graphene on silicon wafers	Introduction of air bubbles during rinsing of PMMA membranes	Air bubbles can be removed by blowing air under the PMMA membranes with a dropper
42	Residual PMMA on the transferred graphene	Too much PMMA dripping during spin coating	Add PMMA dropwise to just cover the copper piece before spin coating
47	The photoresist is not fully spin coated on the device	The surface of the silicon wafer is highly hydrophobic	Treat the spin-coated devices with oxygen plasma for 60 s. Then, remove the photoresist with acetone and spin coat again
59	Poor adhesion of the mark to the silicon wafer	High deposition rate	Reduce the heating current and ensure that the evaporation rate is not higher than $1 \text{ \AA}/10 \text{ s}$
73	The development is incomplete	Short development time or low power of the UV light of lithography	Extend the development time or increase the power of the UV light
82	Graphene FETs are poorly conductive	Poor contact between metal electrodes and graphene	Extend the development time of the electrode pattern or increase the power of the UV light of lithography
92	Etched lines exist only in part of the graphene ribbon	The working distance changes because of stage movement during exposure	Appropriately increase the number of focusing times and focus once every 40 pairs of electrodes
93	The first cutting yield does not reach 50–60%	The etching of graphene is incomplete	Each subsequent cutting time should be judged according to the current decreasing trend. The subsequent cutting time decreases with the decrease in the current until the current reaches the picoampere level
100	Repeat $I-V$ scans show the response of the current	The electroburning of graphene is incomplete	These pairs of electrodes should be excluded when characterizing the single-molecule connection

## Timing

### Preparation of graphene FETs

Steps 1–16, growth of graphene on copper sheets: 4 h

Steps 17–42, transfer of the graphene from the copper sheet to the silicon wafer: 20 h

Steps 43–62, deposition of the mark on the graphene–silicon wafer: 5 h

Steps 63–70, preparation of graphene ribbons: 2 h  
Steps 71–82, preparation of metal electrodes: 5 h

### Preparation of the single-molecule device

Steps 83–92, opening of windows on PMMA layers: 4 h  
Steps 93–96, cutting of graphene ribbons by oxygen plasma: 3 h  
Steps 97–100, supplementary cutting of graphene ribbons by electroburning: 2 h  
Steps 101–106, reconnection of graphene point contacts by molecules: 3 d

## Anticipated results

The single molecule sandwiched between graphene electrodes can be characterized by IETS, single-molecule imaging and single-molecule fluorescent spectra. IETS is the second derivative of the  $I$ – $V$  curve, demonstrating the coupling between electron and phonon. To achieve higher accuracy, IETS can be directly obtained by a lock-in amplifier instrument at 2 K. The second harmonic in the  $I$ – $V$  scan (direct current mode) with (prime-number frequency) alternating current loading is demodulated, namely, IETS. We can compare ( $V = \frac{h\nu}{e}$ ) these spectra with macroscopic or theoretical IR and Raman spectra to find the characteristic peak of the amide bond and its corresponding functional center (Fig. 5 and Supplementary Fig. 10).

To be compatible with the objective lens of an optical characterization system, the chip can be prepared in advance to  $1.8\text{ cm} \times 3.5\text{ cm}$ . Some reaction accompanied by fluorescence blinking can be adopted to determine the single-molecule site<sup>46–48</sup>. After adding the reactant to the loaded reaction cell, we obtain a synchronized pair of optical and electrical signals with strong correlation, showing the connection of the target molecular bridge (Fig. 5). In addition, running the reconstruction algorithm (fitting the Gaussian peak center of each bright spot and overlaying each frame) on the obtained microscopy images allows for identification of the reaction site. The presence of only one bright spot between graphene electrode arrays indicates that there is only one molecular connection (Fig. 4h and more data in Supplementary Fig. 11).

The gate-voltage dependent experiment provides information on the molecular orbital versus the Fermi energy level of the electrode, which is informative of the device's molecular signatures<sup>24,50,63</sup>.

The product catalyzed by the single-molecule catalyst can also be characterized by the fluorescent spectra. For example, the red shift can be recorded during the single-molecule palladium-catalyzed Suzuki-Miyaura cross-coupling, implying that the catalyst works<sup>46</sup> (Fig. 5).

With adequate evidence for a stable (e.g., long time monitoring in Supplementary Fig. 12) single-molecule connection, the inherent properties and anomalous behaviors of molecules (including but not limited to current modulation, energy conversion, hidden intermediate and reaction event correlation) can be detected by suitable temporal resolution, temperature and external stimuli, such as optical, electrical and magnetic fields and chemical reagents (Fig. 1).

### Reporting summary

Further information on research design is available in the Nature Portfolio Reporting Summary linked to this article.

### Data availability

The main data discussed in this protocol are available in the supporting primary research paper<sup>46</sup>. The raw datasets are too large to be publicly shared but are available for research purposes from the corresponding author upon reasonable request.

## References

1. Coontz, R. & Hanson, B. Not so simple. *Science* **305**, 957 (2004).
2. Barkai, E., Jung, Y. J. & Silbey, R. Theory of single-molecule spectroscopy: beyond the ensemble average. *Annu. Rev. Phys. Chem.* **55**, 457–507 (2004).
3. Zrimsek, A. B. et al. Single-molecule chemistry with surface- and tip-enhanced Raman spectroscopy. *Chem. Rev.* **117**, 7583–7613 (2017).
4. Lu, H. P., Xun, L. & Xie, X. S. Single-molecule enzymatic dynamics. *Science* **282**, 1877–1882 (1998).
5. Liu, C. et al. Single polymer growth dynamics. *Science* **358**, 352–355 (2017).
6. Florin, E. L., Moy, V. T. & Gaub, H. E. Adhesion forces between individual ligand-receptor pairs. *Science* **264**, 415–417 (1994).

7. Li, Y., Yang, C. & Guo, X. Single-molecule electrical detection: a promising route toward the fundamental limits of chemistry and life science. *Acc. Chem. Res.* **53**, 159–169 (2020).
8. Xin, N. et al. Concepts in the design and engineering of single-molecule electronic devices. *Nat. Rev. Phys.* **1**, 211–230 (2019).
9. Venkatesan, B. M. & Bashir, R. Nanopore sensors for nucleic acid analysis. *Nat. Nanotechnol.* **6**, 615–624 (2011).
10. Aviram, A. & Ratner, M. A. Molecular rectifiers. *Chem. Phys. Lett.* **29**, 277–283 (1974).
11. Xiang, D., Wang, X., Jia, C., Lee, T. & Guo, X. Molecular-scale electronics: from concept to function. *Chem. Rev.* **116**, 4318–4440 (2016).
12. Li, T., Hu, W. & Zhu, D. Nanogap electrodes. *Adv. Mater.* **22**, 286–300 (2010).
13. Jia, C. & Guo, X. Molecule-electrode interfaces in molecular electronic devices. *Chem. Soc. Rev.* **42**, 5642–5660 (2013).
14. Su, T. A., Neupane, M., Steigerwald, M. L., Venkataraman, L. & Nuckolls, C. Chemical principles of single-molecule electronics. *Nat. Rev. Mater.* **1**, 16002 (2016).
15. Xu, B. & Tao, N. Measurement of single-molecule resistance by repeated formation of molecular junctions. *Science* **301**, 1221–1223 (2003).
16. Venkataraman, L., Klare, J. E., Nuckolls, C., Hybertsen, M. S. & Steigerwald, M. L. Dependence of single-molecule junction conductance on molecular conformation. *Nature* **442**, 904–907 (2006).
17. Reed, M. A., Zhou, C., Muller, C. J., Burgin, T. P. & Tour, J. M. Conductance of a molecular junction. *Science* **278**, 252–254 (1997).
18. Park, H., Lim, A. K. L., Alivisatos, A. P., Park, J. & McEuen, P. L. Fabrication of metallic electrodes with nanometer separation by electromigration. *Appl. Phys. Lett.* **75**, 301–303 (1999).
19. Park, J. et al. Coulomb blockade and the Kondo effect in single-atom transistors. *Nature* **417**, 722–725 (2002).
20. Gehring, P. et al. Field-effect control of graphene–fullerene thermoelectric nanodevices. *Nano Lett.* **17**, 7055–7061 (2017).
21. Burzurí, E. et al. Sequential electron transport and vibrational excitations in an organic molecule coupled to few-layer graphene electrodes. *ACS Nano* **10**, 2521–2527 (2016).
22. Burzurí, E. et al. Spin-state dependent conductance switching in single molecule-graphene junctions. *Nanoscale* **10**, 7905–7911 (2018).
23. Island, J. O. et al. Fabrication of hybrid molecular devices using multi-layer graphene break junctions. *J. Phys. Condens. Matter* **26**, 474205 (2014).
24. Prins, F. et al. Room-temperature gating of molecular junctions using few-layer graphene nanogap electrodes. *Nano Lett.* **11**, 4607–4611 (2011).
25. Lau, C. S. et al. Redox-dependent Franck–Condon blockade and avalanche transport in a graphene–fullerene single-molecule transistor. *Nano Lett.* **16**, 170–176 (2015).
26. Limburg, B. et al. Anchor groups for graphene–porphyrin single-molecule transistors. *Adv. Funct. Mater.* **28**, 1803629 (2018).
27. Mol, J. A. et al. Graphene–porphyrin single-molecule transistors. *Nanoscale* **7**, 13181–13185 (2015).
28. Thomas, J. O. et al. Understanding resonant charge transport through weakly coupled single-molecule junctions. *Nat. Commun.* **10**, 4628 (2019).
29. Pei, T. et al. Exchange-induced spin polarization in a single magnetic molecule junction. *Nat. Commun.* **13**, 4506 (2022).
30. Zhao, S. et al. Charge transport through single-molecule bilayer-graphene junctions with atomic thickness. *Chem. Sci.* **13**, 5854–5859 (2022).
31. Cao, Y. et al. Building high-throughput molecular junctions using indented graphene point contacts. *Angew. Chem. Int. Ed. Engl.* **51**, 12228–12232 (2012).
32. Gu, C. H., Su, D. K., Jia, C. C., Ren, S. Z. & Guo, X. F. Building nanogapped graphene electrode arrays by electroburning. *RSC Adv.* **8**, 6814–6819 (2018).
33. Guo, X. et al. Covalently bridging gaps in single-walled carbon nanotubes with conducting molecules. *Science* **311**, 356–359 (2006).
34. Jia, C. et al. Covalently bonded single-molecule junctions with stable and reversible photoswitched conductivity. *Science* **352**, 1443–1445 (2016).
35. Jia, C., Ma, B., Xin, N. & Guo, X. Carbon electrode–molecule junctions: a reliable platform for molecular electronics. *Acc. Chem. Res.* **48**, 2565–2575 (2015).
36. Xin, N. et al. Stereoelectronic effect-induced conductance switching in aromatic chain single-molecule junctions. *Nano Lett.* **17**, 856–861 (2017).
37. Meng, L. et al. Atomically precise engineering of single-molecule stereoelectronic effect. *Angew. Chem. Int. Ed. Engl.* **60**, 12274–12278 (2021).
38. Yang, C. et al. Complete deciphering of the dynamic stereostructures of a single aggregation-induced emission molecule. *Matter* **5**, 1224–1234 (2022).
39. Wen, H. et al. Complex formation dynamics in a single-molecule electronic device. *Sci. Adv.* **2**, e1601113 (2016).
40. Zhou, C. et al. Direct observation of single-molecule hydrogen-bond dynamics with single-bond resolution. *Nat. Commun.* **9**, 807 (2018).
41. Liu, Z. et al. A single-molecule electrical approach for amino acid detection and chirality recognition. *Sci. Adv.* **7**, eabe4365 (2021).

42. Chen, S. et al. Real-time observation of the dynamics of an individual rotaxane molecular shuttle using a single-molecule junction. *Chem* **8**, 243–252 (2022).
43. Guo, Y., Yang, C., Jia, C. & Guo, X. Accurate single-molecule indicator of solvent effects. *JACS Au* **1**, 2271–2279 (2021).
44. Gu, C. et al. Label-free dynamic detection of single-molecule nucleophilic-substitution reactions. *Nano Lett.* **18**, 4156–4162 (2018).
45. Yang, C. et al. Single-molecule electrical spectroscopy of organocatalysis. *Matter* **4**, 2874–2885 (2021).
46. Yang, C. et al. Unveiling the full reaction path of the Suzuki–Miyaura cross-coupling in a single-molecule junction. *Nat. Nanotechnol.* **16**, 1214–1223 (2021).
47. Yang, C. et al. Electric field-catalyzed single-molecule Diels–Alder reaction dynamics. *Sci. Adv.* **7**, eabf0689 (2021).
48. Guo, Y. et al. Accurate single-molecule kinetic isotope effects. *J. Am. Chem. Soc.* **144**, 3146–3153 (2022).
49. Meng, L. et al. Side-group chemical gating via reversible optical and electric control in a single molecule transistor. *Nat. Commun.* **10**, 1450 (2019).
50. Xin, N. et al. Tuning charge transport in aromatic-ring single-molecule junctions via ionic-liquid gating. *Angew. Chem. Int. Ed. Engl.* **57**, 14026–14031 (2018).
51. Xin, N. et al. Control of unipolar/ambipolar transport in single-molecule transistors through interface engineering. *Adv. Electron. Mater.* **6**, 1901237 (2020).
52. Xin, N. et al. Tunable symmetry-breaking-induced dual functions in stable and photoswitched single-molecule junctions. *J. Am. Chem. Soc.* **143**, 20811–20817 (2021).
53. Stefani, D. et al. Large conductance variations in a mechanosensitive single-molecule junction. *Nano Lett.* **18**, 5981–5988 (2018).
54. Vazquez, H. et al. Probing the conductance superposition law in single-molecule circuits with parallel paths. *Nat. Nanotechnol.* **7**, 663–667 (2012).
55. Greenwald, J. E. et al. Highly nonlinear transport across single-molecule junctions via destructive quantum interference. *Nat. Nanotechnol.* **16**, 313–317 (2020).
56. Zhang, L. et al. Electrochemical and electrostatic cleavage of alkoxyamines. *J. Am. Chem. Soc.* **140**, 766–774 (2018).
57. Venkataraman, L. et al. Electronics and chemistry: varying single-molecule junction conductance using chemical substituents. *Nano Lett.* **7**, 502–506 (2007).
58. Zhang, Y. et al. Distinguishing diketopyrrolopyrrole isomers in single-molecule junctions via reversible stimuli-responsive quantum interference. *J. Am. Chem. Soc.* **140**, 6531–6535 (2018).
59. Su, T. A., Li, H., Steigerwald, M. L., Venkataraman, L. & Nuckolls, C. Stereoelectronic switching in single-molecule junctions. *Nat. Chem.* **7**, 215–220 (2015).
60. Huang, S. et al. Identifying single bases in a DNA oligomer with electron tunnelling. *Nat. Nanotechnol.* **5**, 868–873 (2010).
61. Zhao, Y. et al. Single-molecule spectroscopy of amino acids and peptides by recognition tunnelling. *Nat. Nanotechnol.* **9**, 466–473 (2014).
62. Zhu, J. et al. Solution-processable carbon nanoelectrodes for single-molecule investigations. *J. Am. Chem. Soc.* **138**, 2905–2908 (2016).
63. Xu, Q. et al. Single electron transistor with single aromatic ring molecule covalently connected to graphene nanogaps. *Nano Lett.* **17**, 5335–5341 (2017).
64. Caneva, S. et al. Mechanically controlled quantum interference in graphene break junctions. *Nat. Nanotechnol.* **13**, 1126–1131 (2018).
65. El Abbassi, M. et al. Robust graphene-based molecular devices. *Nat. Nanotechnol.* **14**, 957–961 (2019).
66. Gehring, P. et al. Distinguishing lead and molecule states in graphene-based single-electron transistors. *ACS Nano* **11**, 5325–5331 (2017).
67. Nef, C. et al. High-yield fabrication of nm-size gaps in monolayer CVD graphene. *Nanoscale* **6**, 7249–7254 (2014).
68. Cully, J. J., Swett, J. L., Willick, K., Baugh, J. & Mol, J. A. Graphene nanogaps for the directed assembly of single-nanoparticle devices. *Nanoscale* **13**, 6513–6520 (2021).
69. Lau, C. S., Mol, J. A., Warner, J. H. & Briggs, G. A. D. Nanoscale control of graphene electrodes. *Phys. Chem. Chem. Phys.* **16**, 20398–20401 (2014).
70. Agrawal, S., Raghuvver, M. S., Kroger, R. & Ramanath, G. Electrical current-induced structural changes and chemical functionalization of carbon nanotubes. *J. Appl. Phys.* **100**, 094314 (2006). 21.
71. Ullmann, K. et al. Single-molecule junctions with epitaxial graphene nanoelectrodes. *Nano Lett.* **15**, 3512–3518 (2015).
72. Tincu, B. et al. Investigation of plasma-assisted functionalization of pristine single layer graphene. *Chem. Phys. Lett.* **789**, 139330 (2022).
73. Cao, Y., Dong, S., Liu, S., Liu, Z. & Guo, X. Toward functional molecular devices based on graphene molecule junctions. *Angew. Chem. Int. Ed. Engl.* **52**, 3906–3910 (2013).
74. Imai-Imada, M. et al. Orbital-resolved visualization of single-molecule photocurrent channels. *Nature* **603**, 829–834 (2022).

### Acknowledgements

We acknowledge primary financial support from the National Key R&D Program of China (2021YFA1200101 and 2022YFE0128700), the National Natural Science Foundation of China (22150013, 21727806 and 21933001), the Tencent Foundation through the XPLOERER PRIZE “Frontiers Science Center for New Organic Matter” at Nankai University (63181206) and the Natural Science Foundation of Beijing (2222009).

### Author contributions

Chen Yang, Caiyao Yang and X.G. designed and created the figures. Chen Yang, Caiyao Yang, Y.G. and J.F. performed the experiments and wrote the manuscript. X.G. supervised the research and edited the manuscript.

### Competing interests

The authors declare no competing interests.

### Additional information

**Supplementary information** The online version contains supplementary material available at <https://doi.org/10.1038/s41596-023-00822-x>.

**Correspondence and requests for materials** should be addressed to Xuefeng Guo.

**Peer review information** *Nature Protocols* thanks the anonymous reviewers for their contribution to the peer review of this work.

**Reprints and permissions information** is available at [www.nature.com/reprints](http://www.nature.com/reprints).

**Publisher's note** Springer Nature remains neutral with regard to jurisdictional claims in published maps and institutional affiliations.

Springer Nature or its licensor (e.g. a society or other partner) holds exclusive rights to this article under a publishing agreement with the author(s) or other rightsholder(s); author self-archiving of the accepted manuscript version of this article is solely governed by the terms of such publishing agreement and applicable law.

Received: 20 May 2022; Accepted: 9 February 2023;

Published online: 12 April 2023

### Related links

#### Key references using this protocol

Jia, C. et al. *Science* **352**, 1443–1445 (2016): <https://doi.org/10.1126/science.aaf6298>

Yang, C. et al. *Nat. Nanotechnol.* **16**, 1214–1223 (2021): <https://doi.org/10.1038/s41565-021-00959-4>

Yang, C. et al. *Sci. Adv.* **7**, eabf0689 (2021): <https://doi.org/10.1126/sciadv.abf0689>